Geoinformation Issues
Vol. 9, No 1 (9), 39–51/2017

AVHRR LAC satellite cloud climatology over Central Europe derived by the Vectorized Earth Observation Retrieval (VEOR) method and PyLAC software

Jan Paweł Musiał
Institute of Geodesy and Cartography, 27 Jacka Kaczmarskiego St., 02-679, Warsaw, Poland
Tel.: +48 22 3291984, Fax: +48 22 3291950, E-mail: jan.musial@igik.edu.pl
Jędrzej Stanisław Bojanowski
Institute of Geodesy and Cartography, 27 Jacka Kaczmarskiego St., 02-679, Warsaw, Poland
Tel.: +48 22 3291985, Fax: +48 22 3291950, E-mail: jedrzej.bojanowski@igik.edu.pl

Abstract: The study presents the first edition of cloud coverage and cloud physical properties climate data records (CDRs) over Central Europe compiled from 1 × 1 km resolution AVHRR imagery. The CDRs cover a climatological period of 30 years from 1986 to 2016. The dataset was generated using a novel Vectorized Earth Observation Retrieval (VEOR) algorithm that is an extension of the fast look-up table approach implemented in the Probabilistic Cloud Mask (PCM) method. AVHRR local area coverage (LAC) L1b data were pre-processed to reflectances and brightness temperatures using the PyLAC software, which is a modification of the PyGAC package used to generate CM SAF CLARA-A2 dataset from AVHRR global area coverage (GAC) imagery. The main motivation for the study was the analysis of small scale changes in cloudiness and its physical properties induced by local factors that are not apparent at coarse GAC resolution. A secondary goal was to create a framework for VEOR training against MODIS imagery and MODIS-derived cloud products, and then applying it to data originating from other sensors such as AVHRR.

Keywords: AVHRR, satellite climatology, clouds, cloud properties, CDR, VEOR

Received: 16 January 2018 / Accepted: 9 April 2018

1. Introduction

Cloud radiative forcing and cloud-aerosol interactions are of indisputable importance for understanding climate change. Most of the global climate models operate at a scale of roughly 100 km (Saha et al., 2010; Dee et al., 2011). Such a scale allows an accurate simulation of the mid-latitude weather systems that spread across thousands of kilometres, but it is insufficient to capture convective cloud systems that rarely extend beyond a few tens of kilometres. Therefore, the impact of the convective cloud systems within climate models is approximated by complex parametrizations which incorporate the main source of errors and uncertainties in the simulations. Decreasing the size of the model grid cells to 1 km^2 or less would allow major convective cloud systems to be resolved. Furthermore, such resolution would allow a wide range of local scale analyses, e.g.: aerosol-cloud interactions in the vicinity of emitters, impact of cloudiness change on surface radiation in mountainous regions, relationship between cloudiness and urban heat islands (UHI), etc. Thus, there is a strong demand for the satellite cloud climate data record (CDR) that would match the spatial extent of the convective cells.

The quality of a CDR depends heavily on the homogeneity and accuracy of the input measurement set. In the case of the AVHRR sensor a number of factors – such as 1) multitude of satellite platforms (NOAA and MetOp) affected by orbital drift; 2) instrument degradation; 3) differences in spectral response functions; 4) 1.6 μm and 3.7 μm channel switch – resulted in inhomogeneous time series of radiance measurements. Especially the shortwave channels (at 0.6, 0.8, 1.6 μm) are affected because

they do not feature on-board calibration as longwave channels do (at 3.7, 10.8, 12.0 μm). Therefore, prior to any satellite retrieval using a long record of AVHRR data, a vicarious recalibration of the shortwave channels has to be performed to ensure homogeneity and stability of the radiance measurement within and across different satellite platforms. In the present study the AVHRR calibration coefficients developed within the PATMOS-x climatology (Heidinger et al., 2014) were used.

Once the input data are correctly calibrated the satellite retrieval of physical quantities can be performed. In the case of cloudiness and its characteristics the retrieval can be divided into three steps: 1) cloud discrimination, 2) cloud phase retrieval, and 3) retrieval of the remaining physical quantities (cloud optical depth & effective radius, liquid/ice water path, etc.). Apart from algorithm design, one of the important factors affecting the homogeneity of the derived data record is the stability of ancillary data used during the retrieval. Usually the ancillary data originate from a climate reanalysis of surface meteorological data that themselves feature inhomogeneities due to instrument change/malfunction, expansion of spatial cover and density of measurements, assimilation of new types of data (e.g. satellite data), and many more. Thus, within the present study no ancillary data besides snow cover maps and a static land cover map were used. The data record acquired from the retrieval cannot be considered as a CDR without specific post-processing. It involves diurnal cycle correction of physical quantities in the case of satellites featuring orbital drift, homogeneity tests, and validation against independent data (e.g. SYNOP observations). All of the aforementioned aspects make the satellite CDRs derivation difficult and may result in significant discrepancies between them. In the case of older NOAA platforms (up to NOAA17) significant orbital drift occurred that subsequently resulted in spurious temporal trends in satellite products (Devasthale et al., 2012, Pfeifroth et al., 2012). Depending on the trend type this introduces spurious increase or decrease in values in CDRs and voids further climatological analysis.

Existing AVHRR-based cloud cover CDRs such as ISCCP, PATMOS-x (Heidinger et al., 2014), ESA Cloud_cci CC4CL-AVHRR (Stengel et al., 2017), and CLARA-A2 (Karlsson et al., 2017) are based on the AVHRR Global Area Coverage (GAC) data featuring the reduced spatial resolution. AVHRR GAC data are suitable for global climate models (GCMs), whereas LAC data should be used by regional climate models (RCMs). To date, the 1 km^2 satellite cloud climatology (i.e. 30 years) over Europe has not been compiled. Hence, the main objective of the present study was to provide long and homogeneous time series of cloudiness and its physical properties.

2. AVHRR sensor description

The Advanced Very High Resolution Radiometer (AVHRR) has been operating aboard the suite of NOAA and MetOp polar orbiting satellites maintained by the National Oceanic and Atmospheric Administration (NOAA) since 1978 and by the European Organisation for the Exploitation of Meteorological Satellites (EUMETSAT) since 2006. Its first generation (prior to NOAA7) equipped with 4 channels was soon replaced by the 5-channel AVHRR-2 instrument (NOAA7-14) with the spectral bands centred around 0.6, 0.8, 3.7, 10.8 and 12.0 μm. Complementary to the 3.7 μm channel the third generation (NOAA15 and later, MetOp series) of this sensor is equipped with a 1.6 μm channel but for compatibility at receiving stations both of them operate interchangeably. Channel switching occurs at the illumination transition zone, e.g. 3.7 μm measurements are taken during the night while for the sunlit portion of an orbit channel 1.6 μm is optionally activated (for some satellites e.g. NOAA18, NOAA19 over Europe this channel is always deactivated). Radiances at 1.6 μm include only the solar component of the electromagnetic spectrum whereas at 3.7 μm most of the radiation originates from the Earth's surface with a small contribution of the solar signal. Nevertheless, this reflective part can be retrieved from the 3.7 μm channel by subtracting the thermal component approximated by the 10.8 μm brightness temperature under the assumption of unit emissivity. The AVHRR data are transmitted from the satellite to a ground receiving station in HRPT (high-resolution picture transmission) format (NOAA platforms) or AHRPT (advanced high-resolution picture transmission) format (MetOp platforms) that correspond to either native 1.1 km × 1.1 km resolution called LAC (Local Area Coverage) or re-

duced resolution called GAC (Global Area Coverage). LAC data is not stored aboard a satellite and is acquired only during a receiving station overpass. GAC data, temporarily stored aboard a satellite, cover an entire satellite swath and are periodically dumped at a receiving station located close to the North Pole. To compute the GAC data, four out of every five samples along the scan line are used to compute one average value, and the data from only every third scan line are processed. As a result, the spatial resolution of GAC data near the subpoint is actually 1.1 km × 4.4 km with a 2.2 km gap between pixels across the scan line.

3. AVHRR calibration

AVHRR instrument does not feature an on-board calibration system of shortwave channels (at 0.6, 0.8, 1.6 µm), which have only been calibrated prior to satellite launch. Over the course of years AVHRR radiometers were degrading (especially the early kinds), which resulted in a systematic drop in measured radiance. From the climatological perspective, such an effect introduces spurious trends in time series. Therefore, a vicarious post-launch calibration is required in order to analyse true climate signals. Within the present study, a set of AVHRR vicarious calibration coefficients developed with the PATMOS-x climatology (Heidinger et al., 2010) was used. In order to verify the integrity of AVHRR reflectances a collection of vast radiometrically stable targets (e.g. deserts, ice sheets) is needed. Over Central Europe such targets do not exist and therefore top surfaces of deep convective clouds (DCCs) were selected for this purpose. Discrimination of DCCs was performed for the summertime season only and for the AVHRR pixels complying to the following restrictions: 1) cloud top temperature lower than 220K, 2) pixel not adjacent to cloud boarder, 3) low thermal (below 1K) and low reflectance (below 3%) variance within a 5 × 5 kernel, 4) satellite zenith angle below 30°, and 5) sun zenith angle below 50°. Once the pixels corresponding to DCCs were selected the box plots presenting monthly median values with quartiles and extreme values were generated (Figs 1 and 2). The acquired results prove that PATMOS-x calibration coefficients (Fig. 2) significantly diminish the effect of instrument degradation as compared to standard, pre-launch coefficients (Fig. 1). Furthermore, the impact of AVHRR calibration on cloud optical thickness can be observed in the bottom panels of Figures 1 and 2.

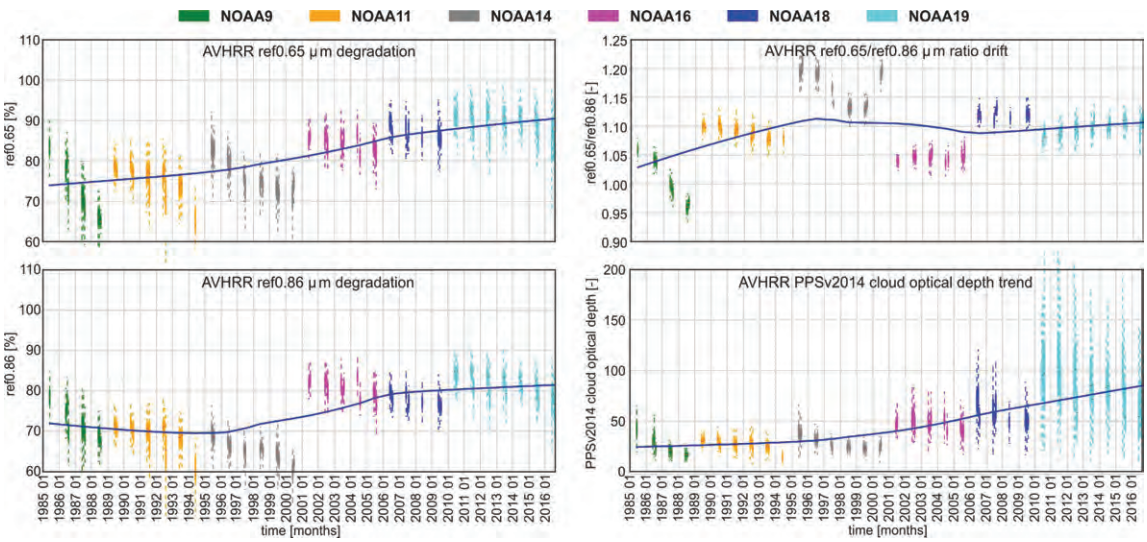

Fig. 1. Box plot with AVHRR reflectance of deep convective clouds featuring standard pre-launch calibration (3 uppermost panels) and derived cloud optical depth by means of the PPSv2014 software (bottom panel); blue line denotes cubic spline fit to data

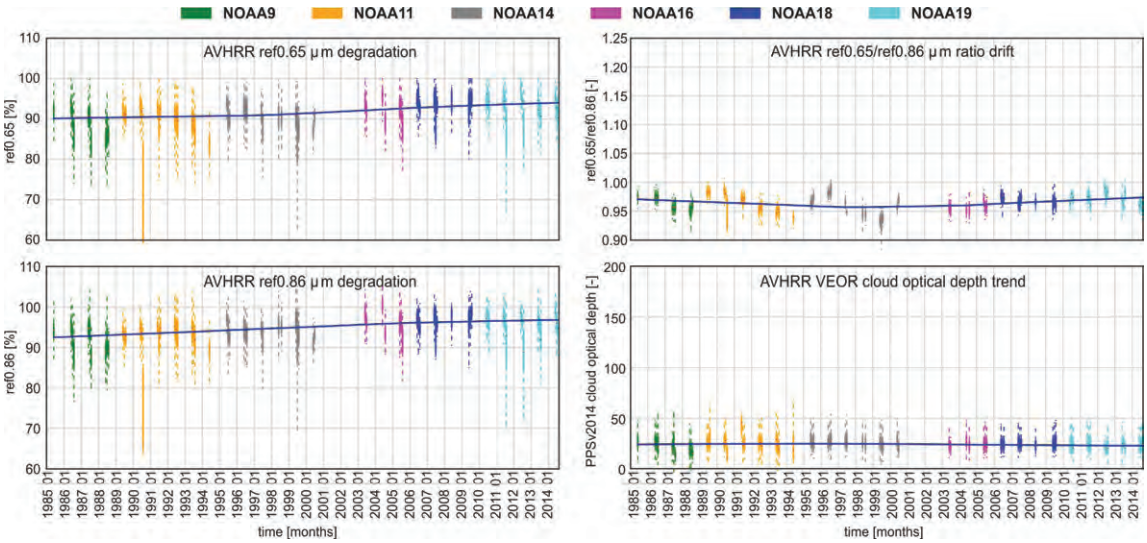

Fig. 2. Box plot with AVHRR reflectance of deep convective clouds featuring PATMOS-x calibration (3 uppermost panels) and derived cloud optical depth by means of the VEOR algorithm (bottom panel); blue line denotes cubic spline fit to data

4. Input data

The data sets used in the study are listed below:

- AVHRR LAC data used to derive CDRs covering the period 1986–2016.
- MODIS and SCIAMACHY data used to spectrally remap MODIS channels to AVHRR bands and to train VEOR algorithm against MODIS cloud products.
- MSG-based CM SAF CLAAS version 2 cloud mean monthly diurnal cycle products used for diurnal cycle correction of the VEOR products. This product features high temporal sampling of 1 hour and covers the European area and therefore was selected for the present study.
- MCD12C1 MODIS annual land cover product at 0.05° spatial resolution.
- NSIDC Northern Hemisphere EASE-Grid 2.0 Weekly Snow Cover and Sea Ice Extent Version 4 (Brodzik and Armstrong, 2013). This data set was derived at 25 km^2 resolution from the following sensors: SMMR, SSM/I, SSMIS, VAS mounted aboard the following platforms: DMSP, DMSP 5D-2/F11, DMSP 5D-2/F13, DMSP 5D-2/F8, DMSP 5D-3/F17, GOES, GOES-7, Nimbus-7. It covers the climatological period from 3 October 1966 to 25 December 2016 which is relevant for the presented study. The ancillary snow dataset is needed to introduce different algorithm parametrization over a bright surface, where the assumption that cloud cover increases measured reflectance is not met. This issue is especially important for cloud masking and cloud optical thickness retrieval, which are mainly based on shortwave reflectance.
- MYD08 collection 6 mean monthly cloud physical properties products at 1° resolution used for inter-comparison with VEOR products.

The AVHRR dataset was composed of raw LAC data in the HRPT format originating from the local receiving station at the Institute of Geodesy and Cartography in Warsaw, Poland combined with the LAC data in the L1b format downloaded from the NOAA CLASS (Comprehensive Large Array-data Stewardship System) archive. To construct the AVHRR dataset a subset of 6 NOAA satellites marked with numbers 9, 11, 14, 16, 18, and 19 was used. The overpass time of these platforms is close to noon local time, which should diminish the effect of the cloudiness diurnal cycle. SCIAMACHY hyperspectral data used in the study consisted of the localized atmospheric spectra in the UV/Vis/NIR/SWIR wavelength range (SCI.NL1P) product.

The SCIAMACHY instrument aboard the ENVISAT platform was designed to perform global measurements of atmospheric trace gases. It featured low spatial resolution (around 26 km × 15 km) and high radiometric resolution (0.2 nm to 1.5 nm) over the range from 240 nm to 1700 nm, and in selected regions between 2000 nm and 2400 nm. High radiometric resolution and free data availability were the key features that justified selection of the SCIAMACHY data in the presented study. The utilized MODIS data incorporated: MYD02 (calibrated radiances), MYD06 (cloud physical properties), MYD35 (cloud mask) collection 6 products originating from the AQUA satellite with afternoon overpass time. MODIS data sets were selected for the present study because they are retrieved using state-of-the-art algorithms which have been improving for the last 20 years. Furthermore, MODIS instruments feature on-board calibration of shortwave and longwave channels, which significantly reduces problems with sensor degradation apparent in the AVHRR time series.

5. Methods

The methodology applied in the study consisted of 4 major steps and is presented in Figure 3.

Within the first step a suite of spectral response functions of the MODIS instrument on board the EOS2 (AQUA) satellite (Fig. 4) and the AVHRR instrument on board the NOAA19 satellite (Fig. 5) were integrated over one year of hyperspectral SCIAMACHY reflectance data.

As a result a set of collocated synthetic AVHRR and MODIS shortwave channels was derived. Further, the synthetic bands were used to train the VEOR algorithm in order to spectrally remap MODIS channels to the AVHRR 0.6 µm and 0.8 µm bands. In the second processing step MODIS reflectances derived from the MYD02 l1b product were remapped to synthetic AVHRR bands. Then, the synthetic AVHRR bands together with 1) MODIS cloud mask (MYD35), 2) MODIS cloud physical properties product (MYD06), 3) MODIS landcover (MCD12C1), and 4) NSIDC snow cover, were used to train the VEOR algorithm. This allowed the derivation of MODIS-like cloud products out of AVHRR imagery in the third processing step. It began with conversion of the raw AVHRR HRPT data format

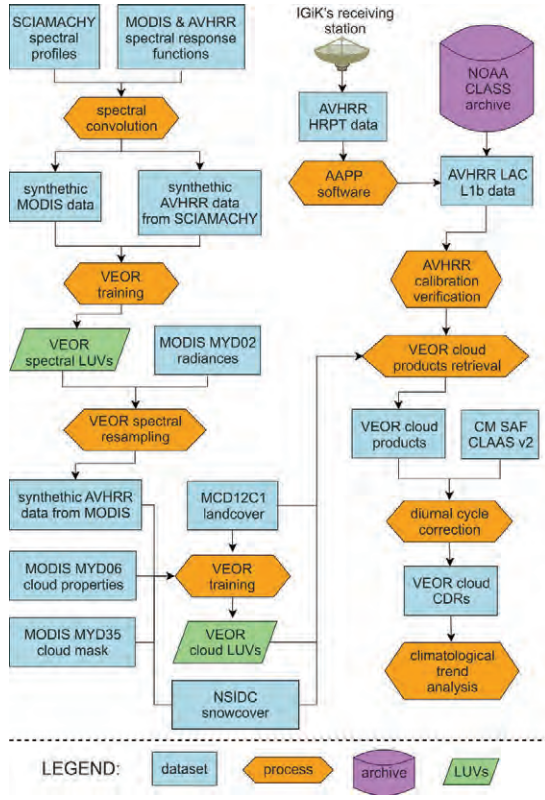

Fig. 3. Flowchart of data processing applied in the study

and NOAA L1b data into the internal L1b format of the NWP SAF AAPP software. Additionally, geolocation of AVHRR imagery, which is affected by satellite clock error and attitude variations, was improved by means of the ANA software (Brunel & Marsouin, 2000). Further, radiometric calibration of AAPP L1b files using the PATMOS-x coefficients was performed by means of the PyLAC software, which stems from the PyGAC package (part of the PyTROLL framework) developed by the CM SAF for the CLARA-A2 dataset. Acquired calibrated reflectances and brightness temperatures were then employed by the VEOR to derive AVHRR cloud products and by the PPSv2014 to derive the Cloud Top Height product. In the last fourth step, the VEOR cloud products were aggregated into monthly averages whenever at least 15 satellite overpasses were available per month. Next, mean monthly diurnal cycle products from the CM SAF CLAAS dataset were bi-linearly resampled to 1 km^2 resolu-

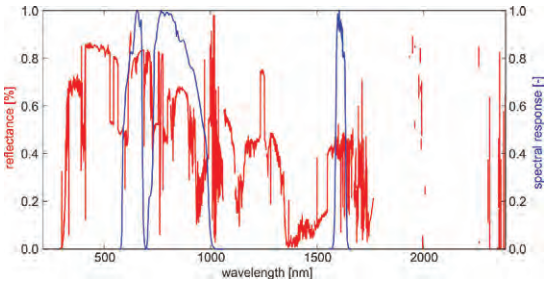

Fig. 4. Spectral response functions of the AVHRR instrument on board the NOAA19 satellite

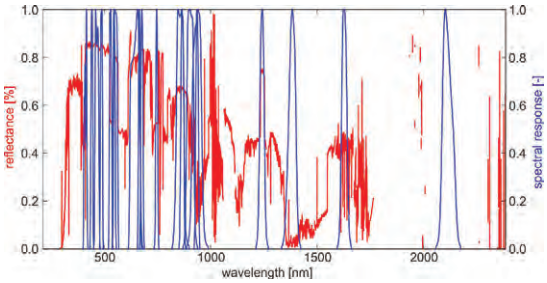

Fig. 5. Spectral response functions of the MODIS instrument on board the AQUA satellite

tion and further averaged to the multiannual means. Then, the diurnal cycle correction factors for each pixel and each month were derived by dividing all hourly values by the value at noon. The correction factors matching the monthly mean NOAA satellites' overpass time were further multiplied by the VEOR cloud products in order to produce diurnally corrected monthly mean cloud CDRs. Ultimately, the following analyses were performed to evaluate the usability of the generated CDRs: 1) temporal changes in cloudiness and its properties averaged over central Europe, 2) mean multiannual distribution of cloudiness and its properties, and 3) spatio-temporal trends of cloudiness and its properties.

VEOR: The Vectorized Earth Observation Retrieval (VEOR) algorithm is a successor of the Probabilistic Cloud Mask (PCM) algorithm (Musial et al., 2014a), which has been successfully applied to AVHRR data for cloud and snow masking and for low stratiform cloud detection (Musial et al., 2014b). Generic formulation of the VEOR retrieval scheme allows its methodology to be extended to a wide range of cloud physical properties such as cloud optical depth, cloud droplet effective radius, cloud physical state, and ice/liquid water path. VEOR processing time is significantly shorter than that of existing methods (e.g. NWC SAF PPS software) due to the implementation of the Look-Up Vectors (LUVs) which describe the position of a pixel within a multidimensional sparse information space composed of spectral, angular and ancillary data. Once the position of a pixel is known it serves as an index to retrieve values from other LUVs that hold precomputed data, e.g. cloud optical depth estimates. In order to generate LUVs with indexes, first continuous data (such as spectral channels) are transformed into a discrete form (unsigned integer values) by means of step functions (Musial et al., 2014b). Further, discrete values originating from different features (spectral channels, ancillary data) are merged into a single value using a bitwise operation. This involves bit shifting and multiplication (bitwise AND operator) in order to locate different features at different bit locations/bit ranges. Once all of the input data sets are converted to a single value then a LUV with mean quantity of interest (e.g. cloud effective radius) is derived by averaging all pixels from the entire training dataset with the same index value. During VEOR retrieval, input data sets are again merged into single index values that are further located within a training LUV by means of a fast binary search algorithm. Ultimately, knowing the position of pixels within the training LUVs the quantity of interest is retrieved.

PyLAC: The PyLAC software implemented in the Python programming language stems from the PyGAC package, part of the PyTROLL framework (https://github.com/pytroll), developed within the CM SAF for the CLARA-A2 dataset. The PyLAC processing chain consists of the following modules: 1) ingestion of an AAPP l1b file, 2) calibration of AVHRR radiances to reflectances and brightness temperatures, 3) geolocation of the satellite scene with the aid of the external binary ANA software (Brunel and Marsouin, 2000) and computation of viewing/Sun angles, 4) remapping of the ancillary data to satellite swath projection, 5) VEOR cloud products retrieval, 6) remapping of AVHRR data and VEOR products to geographic projection, and 7) export of the acquired data to HDF5 format. AVHRR spectral bands utilized for the generation of the cloud products are listed below:

– cloud mask: 0.6, 0.8, 3.7, 10.8 and 12.0 µm bands;
– cloud optical depth: 0.6 µm band;
– cloud effective radius: 3.7 µm band;
– cloud top height (PPSv2014): 10.8 and 12.0 µm bands.

6. Results

Generated VEOR cloud CDRs consist of the following products computed for all types of clouds and with a distinction between ice and water clouds: cloud mask (derived separately for all pixels and for pixels where physical properties retrieval was performed), Cloud Effective Radius (CER) using 3.7 µm band, Cloud Optical Thickness (COT), Ice Water Path (IWP), and Liquid Water Path (LWP). Additionally to VEOR data sets, the Cloud Top Height CDR was generated by means of the PPSv2014 software. All of the aforementioned CDRs cover a period from January 1986 to December 2016 and are projected to the equirectangular coordinate system EPSG:4326 with spatial resolution of $0.01^{o} \times 0.01^{o}$. Aggregated level 3 products in hdf5 format such as decadal trends and mean multiannual CDRs are available online at: http://sonata.igik.edu.pl/#/projects?scrollTo=data#data. In this paper only a subset of VEOR CDRs featuring a statistically significant trend (p-value<0.05) is presented in order to verify acquired results against general knowledge and MYD08 collection 6 mean monthly cloud product.

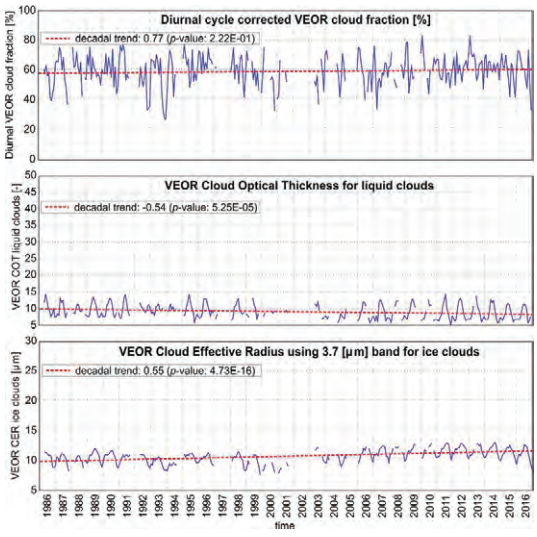

Fig. 6. Time series and temporal trends of selected VEOR cloud products; linear trends were computed using least-squares regression and statistical significance (p-value) was provided by the Wald Test with t-distribution

6.1. Temporal changes in cloudiness and its properties averaged over Central Europe

To analyse a general climatic trend in cloudiness and cloud properties a mean monthly averages over the entire Central Europe were computed (Figs 6 and 7). Apparent data gaps in the presented time series are related to months where fewer than 15 satellite overpasses were available, and to the period 2001–2003 when NOAA16 was not acquiring images at the 3.7 µm band. Performed analyses revealed the following:

1) cloud fraction, liquid cloud optical thickness, and cloud top height, do not feature a statistically significant trend;
2) ice and liquid cloud droplets' effective radius, ice water path, and fraction of liquid clouds, feature a statistically significant positive trend;
3) fraction of ice clouds, liquid water path, optical thickness of liquid clouds, feature statistically significant negative trend;

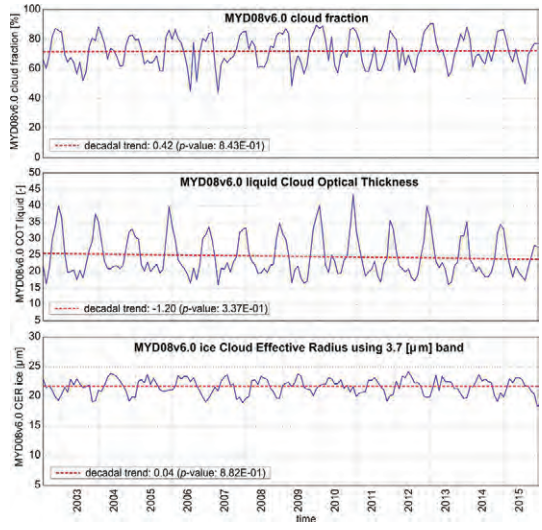

Fig. 7. Time series and temporal trends of selected MYD08v6.0 cloud products; linear trends were computed using least-squares regression and statistical significance (p-value) was provided by the Wald Test with t-distribution

4) comparison of VEOR data with MYD08 collection 6 cloud fraction and cloud optical depth products revealed significant differences in annual cycles; annual cycles of cloud effective radius product are in good agreement.
5) all of the VEOR cloud products feature a lower magnitude of values than MYD08 collection 6 data.

Discrepancies observed between VEOR and MYD08 collection 6 products (Table 1) are related to a different treatment of partially cloudy pixels which are included in the VEOR product and excluded from the MYD08 product. This results in a lower magnitude of VEOR retrievals. Regarding the differences in the annual cycle of cloudiness and some cloud properties, this issue might correspond to a different temporal aggregation methodology as well as a different selection of pixels used in the retrieval. More in depth inter-comparison and validation of VEOR products is beyond the scope of this study and will be included in a subsequent manuscript.

Table 1. Statistics of differences between selected VEOR and MYD08 collection 6 products

Product	Bias	STD	RMSE	Bias corr. RMSE
Cloud fraction [%]	–16.2	17.8	5.8	3.2
Cloud effective radius [μm]	–4.00	3.57	28.78	12.79
Cloud optical depth [-]	–12.87	10.37	27.33	10.76

6.2. Spatial distribution of temporal trends and mean annual products

Spatial distribution and temporal changes in cloud properties were investigated by averaging monthly mean values (Figs 8 and 10) and by computing temporal trends (Figs 9 and 11) from monthly mean products.

Conducted analyses revealed different spatial patterns of cloudiness and cloud properties over Central Europe. Cloud fraction features a distinct pattern with higher values over land than over sea and with a longitudinal negative gradient from West to East. Significantly higher cloud amounts are reported for mountainous regions, which is related to strong convection at mountain tops and to misclassification of snow and cloud covers. Statistically significant temporal trends of cloud fraction are almost exclusively positive in a range of 0.01–0.03% per decade. Cloud optical thickness does not exhibit a strong spatial pattern apart from mountainous regions. However, it has a statistically significant negative North-Western trend of 0.5–1.5 per decade. Cloud effective radius (CER) features higher values over the Adriatic and Ligurian Sea, which might be related to high evaporation combined with a lower amount of available cloud condensation nuclei (CCN). Another region of high CER values is located over the Alps. This might be caused by high ice clouds formed due to strong convection induced by orography. Furthermore, almost all regions exhibit a statistically significant positive temporal trend in CER of a magnitude ranging from 0.5 μm to 2 μm per decade. Cloud ice water paths (IWP) exhibit weak spatial patterns apart from mountainous regions, which again might be related to snow/cloud cover misclassification. Temporal IWP trends feature positive values ranging from 10 to 25 g/m^2 in the South-Eastern part of Central Europe. In contrast, the cloud liquid water path (LWP) reveals a statistically significant negative trend in North-Western regions. Cloud top height (CTH) retrieved by the PPSv2014 algorithm exhibits higher values in the southern part of Central Europe, especially in the foothills of the Alps (Padan Plain) due to higher air temperature and complex orography. Statistically significant CTH trends of 200–400 m per decade exist mostly over the Adriatic and Ligurian Sea. Ultimately, it was found that there is no apparent correlation between local spatial patterns of cloud physical properties and localization of major cities.

7. Conclusions

The present study describes the first edition of cloud cover and physical properties climatic data records (CDRs) at 1 km^2 resolution covering 30 years (1986–2016) retrieved from AVHRR imagery by means of the Vectorized Earth Observation Retrieval (VEOR) algorithm. The primary objective of the study was to investigate local changes in cloudiness that are not apparent at coarse global

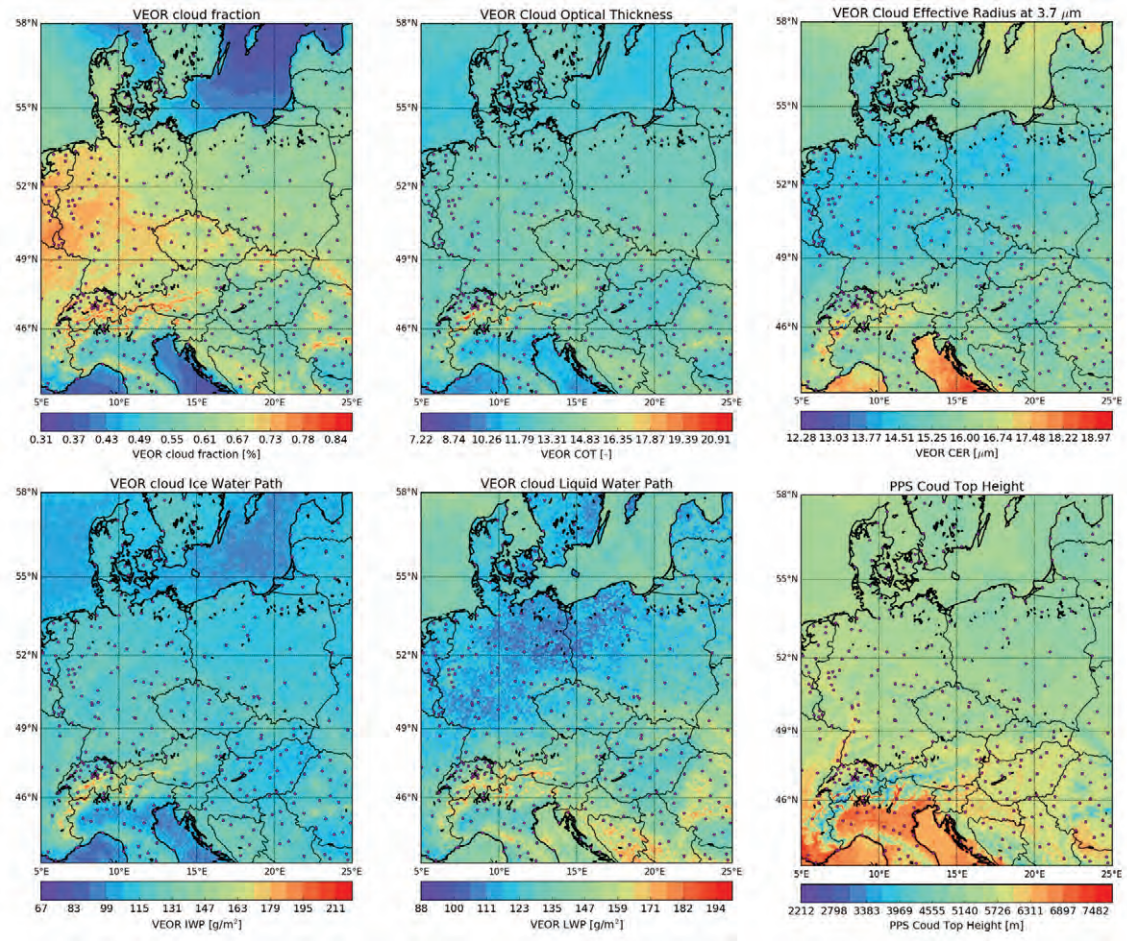

Fig. 8. Multiannual means (1988–2016) of cloud products; purple dots represent major cities

scale. A secondary goal was to create a framework for VEOR training against MODIS imagery and MODIS-derived cloud products, and then apply it to data originating from other sensors such as AVHRR. This framework required spectral resampling of MODIS bands into synthetic AVHRR channels, which was done by another VEOR instance trained against SCIAMACHY hyperspectral data. Despite different AVHRR sensors operating within 30 years, generated VEOR cloud products are relatively consistent and homogeneous due to specific AVHRR channel calibration derived within the PATMOS-x project for the sake of climatological analyses. Furthermore, the quality of VEOR CDRs was improved by correcting for the cloudiness diurnal cycle effect, induced by the orbital drift of the NOAA satellites, using the MSG-based CM SAF CLAAS cloud products. Ultimately, usability of VEOR cloud CDRs for climate studies was briefly evaluated. It was found that the most apparent local spatial patterns of cloudiness exist in regions with rough topography (i.e. the Alps), and that these patterns do not seem to be related to urban areas characterized by a high amount of cloud condensation nuclei (CCN). However, to reveal such patterns more in-depth analysis with a distinction between different cloud types is required. The VEOR cloud CDRs feature statistically significant temporal trends (e.g. in cloud droplet effective radius) that are recommended for further investigation. Moreover, it is planned to compare VEOR cloud CDRs with other existing data sets such as MODIS cloud pro-

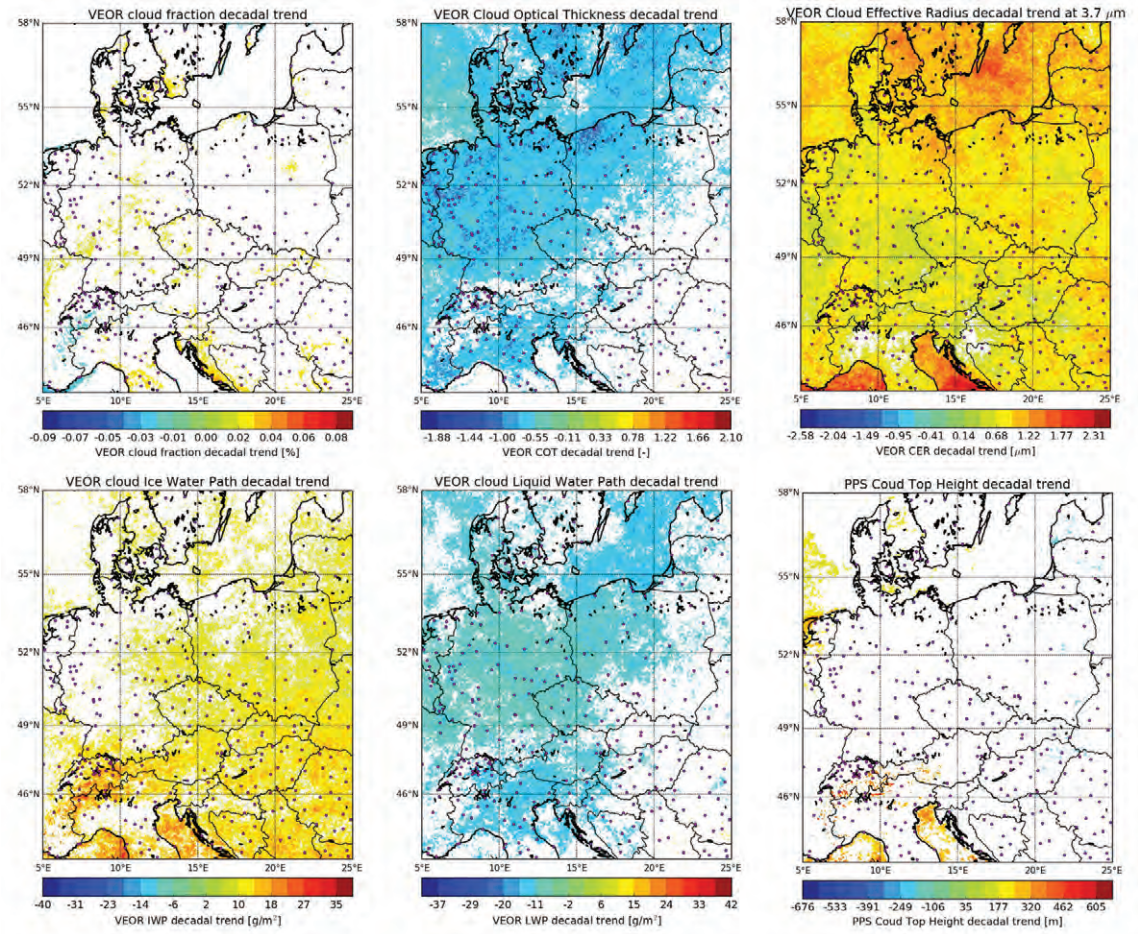

Fig. 9. Temporal linear trends (1988–2016) of cloud products computed using least-squares regression; white background denotes regions where trends were not statistically significant according to the Wald Test with *t*-distribution (*p*-value>0.05); purple dots represent major cities

ducts, CLARA-A2 and PATMOS-x cloud climatologies. The second, more complete edition of VEOR cloud CDRs is expected to be generated after the release of the AVHRR LAC data within the European Space Agency (ESA) Long Term Data Preservation (LTDP) project.

Acknowledgements

The study was financed by the National Science Centre of Poland within the research grants: 1) No DEC-2013/11/D/ST10/03487, and 2) No 2015/19/P/ST10/03990 that received funding from the European Union's Horizon 2020 research and innovation programme under the Marie Sklodowska-Curie grant agreement No 665778. Authors would like to gratefully acknowledge the following: the National Aeronautics and Space Administration (NASA) for providing MODIS data, the National Oceanic and Atmospheric Administration (NOAA) for providing AVHRR data, the European Space Agency (ESA) for providing the SCIAMACHY data, and the National Snow and Ice Data Center (NSIDC) for providing snow cover data. This research was carried out with the support of the Interdisciplinary Centre for Mathematical and Computational Modelling (ICM) University of Warsaw under grant No GB69-1.

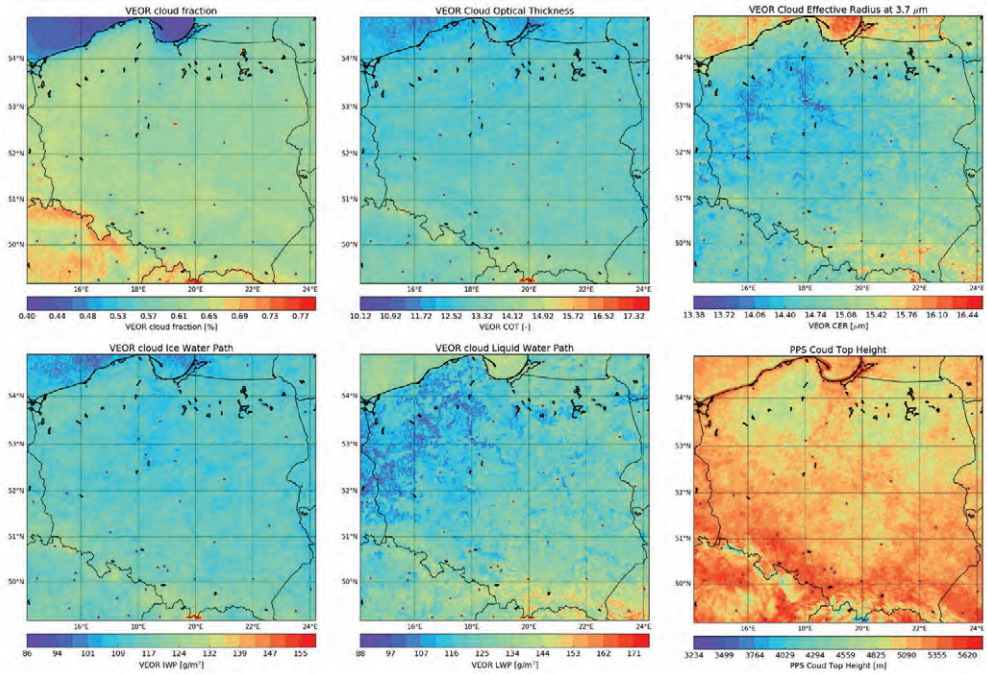

Fig. 10. Multiannual means (1988–2016) of cloud products; purple dots represent major cities

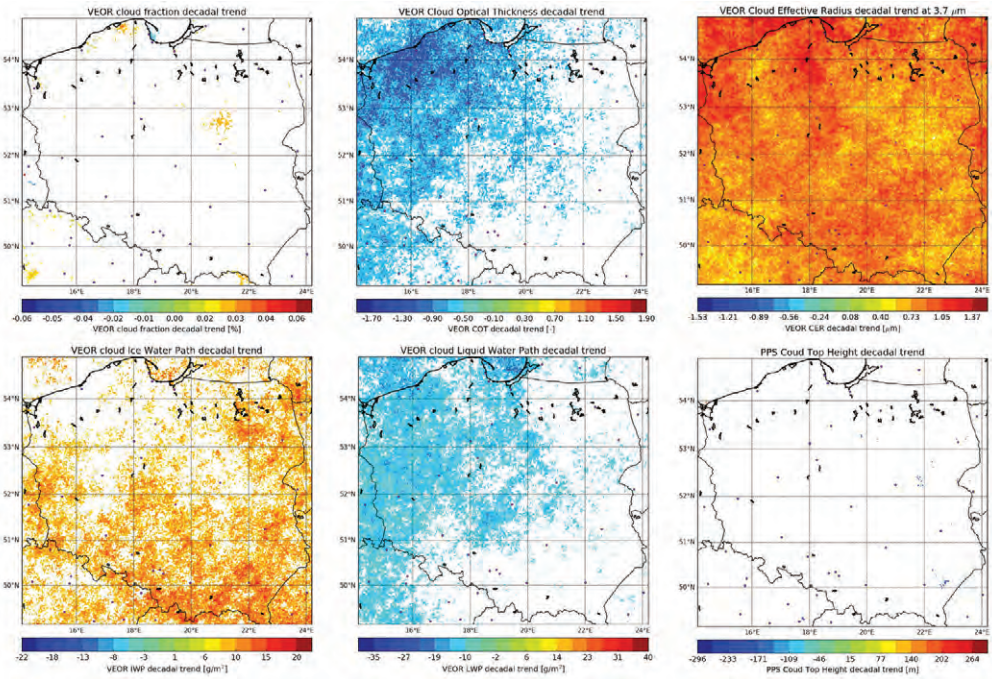

Fig. 11. Temporal linear trends (1988–2016) of cloud products computed using least-squares regression; white background denotes regions where trends were not statistically significant according to the Wald Test with *t*-distribution (*p*-value>0.05); purple dots represent major cities

References

Benas N., Finkensieper S., Stengel M., van Zadelhoff G.J., Hanschmann T., Hollmann R., Meirink J.F., (2017): *The MSG-SEVIRI-based cloud property data record CLAAS-2*, Earth System Science Data, 9(2), pp. 415–434, https://doi.org/10.5194/essd-9-415-2017

Brodzik M., Armstrong R., (2013): *Northern Hemisphere EASE-Grid 2.0 Weekly Snow Cover and Sea Ice Extent. Version 4. National Snow and Ice Data Center*, Boulder, CO, https://doi.org/10.5067/P7O0HGJLYUQU

Brunel P., Marsouin A., (2000): *Operational AVHRR navigation results*, International Journal of Remote Sensing, 21(5), pp. 951–972, https://doi.org/10.1080/014311600210371

Dee D.P., Uppala S.M., Simmons A.J., Berrisford P., Poli P., Kobayashi S., Bechtold P., (2011): *The ERA-Interim reanalysis: Configuration and performance of the data assimilation system*, Quarterly Journal of the Royal Meteorological Society, 137(656), pp. 553–597, DOI 10.1002/qj.828

Devasthale A., Karlsson K.G., Quaas J., Graßl H., (2012): *Correcting orbital drift signal in the time series of AVHRR derived convective cloud fraction using rotated empirical orthogonal function*, Atmospheric Measurement Techniques, 5(2), pp. 267–273.

Heidinger A.K., Straka III W.C., Molling C.C., Sullivan J.T., Wu X., (2010): *Deriving an inter-sensor consistent calibration for the AVHRR solar reflectance data record*, International Journal of Remote Sensing, 31(24), pp. 6493–6517, doi.org/10.1080/01431161.2010.496472

Heidinger A.K., Foster M.J., Walther A., Zhao X., (2014): *The pathfinder atmospheres–extended AVHRR climate dataset*, Bulletin of the American Meteorological Society, 95(6), pp. 909–922, https://doi.org/10.1175/BAMS-D-12-00246.1

Karlsson K.G., Anttila K., Trentmann J., Stengel M., Meirink J.F., Devasthale A., Hanschmann T., Kothe S., Jääskeläinen E., Sedlar J., Benas N., van Zadelhoff G.J., Schlundt K., Stein D., Finkensieper S., Håkansson N., Hollmann R., (2017): *CLARA-A2: the second edition of the CM SAF cloud and radiation data record from 34 years of global AVHRR data*, Atmospheric Chemistry and Physics, 17(9), pp. 5809–5828.

Kästner M., Kriebel K.T., (2001): *Alpine cloud climatology using long-term NOAA-AVHRR satellite data*, Theoretical and Applied Climatology, 68(3–4), pp. 175–195, https://doi.org/10.1007/s007040170044

Meerkötter R., König C., Bissolli P., Gesell G., Mannstein H., (2004): *A 14-year European Cloud Climatology from NOAA/AVHRR data in comparison to surface observations*, Geophysical Research Letters, 31(15), pp. 15103–15107, doi:10.1029/2004GL020098

Musial J.P., Hüsler F., Sütterlin M.B., Neuhaus C., Wunderle S., (2014): *Probabilistic approach to cloud and snow detection on Advanced Very High Resolution Radiometer (AVHRR) imagery*, Atmospheric Measurement Techniques (AMT), 7(3), pp. 799–822, https://doaj.org/article/b84ec2503d9f49fb849b27652151ccda

Musial J.P., Hüsler F., Sütterlin M., Neuhaus C., Wunderle S., (2014): *Daytime low stratiform cloud detection on AVHRR imagery*, Remote Sensing, 6(6), pp. 5124–5150, doi:10.3390/rs6065124

Pfeifroth U., Hollmann R., Ahrens B., (2012): *Cloud cover diurnal cycles in satellite data and regional climate model simulations*, Meteorologische Zeitschrift, 21(6), pp. 551–560, DOI: 10.1127/0941-2948/2012/0423

Saha S., Moorthi S., Pan H.L., Wu X., Wang J., Nadiga S., Liu H., (2010): *The NCEP climate forecast system reanalysis*, Bulletin of the American Meteorological Society, 91(8), pp. 1015–1058, https://doi.org/10.1175/2010BAMS3001.1

Stengel M., Stapelberg S., Sus O., Schlundt C., Poulsen C., Thomas G., Christensen M., Henken C.C., Preusker R., Fischer J., Devasthale A., Willén U., Karlsson K.-G., McGarragh G.R., Proud S., Povey A.C., Grainger R.G., Meirink J.F., Feofilov A., Bennartz R., Bojanowski J.S., Hollmann R., (2017): *Cloud property datasets retrieved from AVHRR, MODIS, AATSR and MERIS in the framework of the Cloud_cci project*, Earth System Science Data, 9, pp. 881–904, https://www.earth-syst-sci-data.net/9/881/2017/

Satelitarna klimatologia chmur wyznaczona z danych AVHRR LAC nad Europą Centralną za pomocą algorytmu Vectorized Earth Observation Retrieval (VEOR) i oprogramowania PyLAC

Jan Paweł Musiał
Instytut Geodezji i Kartografii, ul. Jacka Kaczmarskiego 27, 02-679, Warszawa
Tel.: +48 22 3291984, Fax: +48 22 3291950, E-mail: jan.musial@igik.edu.pl

Jędrzej Stanisław Bojanowski
Instytut Geodezji i Kartografii, ul. Jacka Kaczmarskiego 27, 02-679, Warszawa
Tel.: +48 22 3291985, Fax: +48 22 3291950, E-mail: jedrzej.bojanowski@igik.edu.pl

Streszczenie: Opracowanie prezentuje pierwszą wersję klimatycznego zestawu danych (ang. CDR) opisującego zachmurzenie i jego właściwości fizyczne nad Centralną Europą stworzonego na podstawie danych AVHRR local area coverage (LAC) o rozdzielczości przestrzennej 1 km × 1 km. Zakres opisywanego zestawu danych obejmuje przedział czasowy od 1986 do 2016 roku. Został on wygenerowany przy użyciu nowatorskiego algorytmu Vectorized Earth Observation Retrieval (VEOR), który jest modyfikacją istniejącej Probabilistic Cloud Mask (PCM). Zobrazowania AVHRR w formacie L1b zostały wstępnie przetworzone do reflektancji i temperatur radiacyjnych za pomocą autorskiego oprogramowania PyLAC, które jest modyfikacją oprogramowania PyGAC, dostarczonego w ramach projektu CLARA-A2 przez EUMETSAT CM SAF. Głównym celem opracowania była analiza małoobszarowych zmian zachmurzenia i jego właściwości fizycznych, które nie są widoczne na niskorozdzielczych obrazach AVHRR global area coverage (GAC). Drugorzędnym celem było opracowanie metodologii opartej na algorytmie VEOR, która pozwalała by na powielanie produktów satelitarnych MODIS na innych sensorach takich jak AVHRR.

Słowa kluczowe: AVHRR, klimatologia satelitarna, chmury, właściwości chmur, CDR, VEOR